The Effect of Electrical Polarization on Electronic Structure in LSM Electrodes: An Operando XAS, RIXS and XES Study

Traulsen, Marie Lund; Carvalho, H.W.P.; Zielke, Philipp; Grunwaldt, J.-D.

Published in:
Journal of The Electrochemical Society

Link to article, DOI:
10.1149/2.0091710jes

Publication date:
2017

Document Version
Publisher's PDF, also known as Version of record

JES Focus Issue on Oxygen Reduction and Evolution Reactions for High Temperature Energy Conversion and Storage

The Effect of Electrical Polarization on Electronic Structure in LSM Electrodes: An Operando XAS, RIXS and XES Study

M. L. Traulsen,[a,z] H. W. P. de Carvalho,[b,d] P. Zielke,[a] and J. -D. Grunwaldt[b,c]

[a]*Department of Energy Conversion and Storage, Technical University of Denmark, 4000 Roskilde, Denmark*
[b]*Institute for Chemical Technology and Polymer Chemistry, Karlsruhe Institute of Technology, 76131 Karlsruhe, Germany*
[c]*Institute of Catalysis Research and Technology, Karlsruhe Institute of Technology, 76344 Eggenstein-Leopoldshafen, Germany*

The influence of electrical polarization on Mn in $La_{0.5}Sr_{0.5}MnO_{3\pm\delta}$ electrodes has been investigated by operando High Energy Resolved Fluorescence Detected X-Ray Absorption Near-Edge Structure (HERFD-XANES) spectroscopy, Kβ X-ray Emission Spectroscopy (XES) and Resonant Inelastic X-ray Scattering (RIXS) at the Mn K-edge. The study of polarization induced changes in the electronic properties and structure has been carried out at 500°C in 10–20% O_2 with electrical polarization applied in the range from −850 mV to 800 mV. Cathodic polarizations in the range −600 mV to −850 mV induced a shift in the Mn K edge energy towards lower energies. The shift is assigned to a decrease in the average Mn oxidation state, which based on Kβ XES changes from 3.4 at open circuit voltage to 3.2 at −800 mV applied potential. Furthermore, RIXS rendered pronounced changes in the population of the Mn 3*d* orbitals, due to filling of the Mn *d*-orbitals during the cathodic polarization. Overall, the study experimentally links the electrical polarization of LSM electrodes to the structural and electronic properties of Mn - these properties are expected to be of major importance for the electrocatalytic performance of LSM electrode towards the oxygen reduction reaction.

Manuscript submitted April 3, 2017; revised manuscript received June 15, 2017. Published July 1, 2017. *This paper is part of the JES Focus Issue on Oxygen Reduction and Evolution Reactions for High Temperature Energy Conversion and Storage.*

In high temperature solid oxide electrolysis and solid oxide fuel cells LSM has for decades been a common choice for application in the oxygen electrode.[1] The popularity of LSM based electrodes is mainly due to the LSM's high electronic conductivity, the material's good chemical stability and thermal compatibility with other cell materials and last, but not least, the electrocatalytic activity of LSM towards the oxygen evolution reaction (OER) and the oxygen reduction reactions (ORR).[1,2] The complex defect chemistry of LSM and the materials electrocatalytic properties has been investigated and discussed for long, and it is well-established that the interplay between the electrical polarization and the LSM's electronic structure strongly influences the electrocatalytic properties of the material. However, extensive experimental studies of this interplay at realistic operating conditions, i.e operando studies, have been scarce.

From earlier experimental work it is known, that the creation of oxygen vacancies and accompanying charge compensation mechanism is relevant for the electrocatalytic properties of LSM electrodes, as oxygen vacancies are formed during the cathodic polarization of the electrodes. Hammouche et al.[3] concluded from electrochemical characterization and thermogravimetry that the electrocatalytic properties of LSM for reduction of oxygen were closely related to the generation of oxide vacancies inside the material. Concordingly the highest electrocatalytic activity was observed for LSM50, which had the maximum level of Sr dopant, and thus the highest level of oxygen vacancies, of the investigated compounds.[3] Lee et al.[4] used in situ XPS and electrochemical studies to prove that the cathodic polarization decreased the Mn oxidation state and led to formation of oxygen vacancies. These surface oxygen vacancy sites together with triple phase boundary sites were assumed to be active in the oxygen reduction.[4] The experimental findings summarized so far all point in the direction that the oxygen reduction reaction on LSM may be strongly enhanced during cathodic polarization due to the formation of oxygen vacancies and the correlated reduction in manganese oxidation state.

On the theoretical side, Pavone et al.[5] recently reported DFT calculations predicting the Mn oxidation state during operation of LSM electrodes. Pavone et al.[5] concluded that for LSM50 all Mn^{4+} ions would be reduced to Mn^{3+} ions during operation prior to any further reduction to Mn^{2+}, while in $LaMnO_3$ and $La_{0.75}Sr_{0.25}MnO_3$ (LSM25) both reduction from Mn^{3+} to Mn^{2+} and from Mn^{4+} to Mn^{3+} could occur concurrently. In contrast to this, the work by Mizusaki et al.[6] based on thermogravimetric studies and defect modelling predicts that in LSM50 Mn^{4+}, $Mn^{3+}$and Mn^{2+} will be present simultaneous at the operating conditions, i.e. during electrical polarization at elevated temperatures in oxygen-containing atmosphere. The discrepancies in the theoretical predictions on the Mn oxidation states in LSM50 thus require experiments unravelling the electronic structure around Mn in operating LSM50 electrodes.

As the LSM operate at elevated temperature in ambient pressure and during electrical polarization, the number of applicable techniques for studying the electronic structures is limited. In situ XPS has been applied by several groups in order to obtain knowledge on surface composition and oxidation states[4,7,8] and also in situ STM has been employed to study electronic properties on LSM electrodes.[9] A recent in situ study by Mueller et al.[10] on lanthanum ferrite electrodes did employ X-ray absorption spectroscopy at 1 mbar oxygen partial pressure and revealed a close interplay between transition metals and oxygen ions in the electrode surface during electrical polarization. All these in situ studies yield important information regarding the surface state of the electrodes, but in all cases the studies have been conducted at oxygen partial pressures significantly lower than ambient pressure.

The present study tries to bridge the pressure gap by applying hard X-ray absorption spectroscopy and X-ray emission spectroscopy on an LSM electrode operating at ambient pressure. Thus we consider this an operando study as both pressure, temperature and electrical polarization during the experiments are held at values similar to those experienced at real operation of LSM electrodes. The approach described herein yields information on the bulk electronic properties in the electrodes, and thus complements the previously mentioned surface studies. The advantage is that by using hard X-rays one can really conduct operando studies as hard X-rays can penetrate window materials and the gas phase. In future, the use of hard X-rays may be extended to even more surface sensitive methods such as

[d]Present address: Centro de Energia Nuclear na Agricultura, Universidade de São Paulo, Piracicaba, Brazil.
[z]E-mail: matr@dtu.dk

grazing incidence methods, which will yield information specific for the surface which is the final origin of the electrocatalytic performance. With respect to LSM electrodes only very few attempts have so far been briefly reported on conducting operando XAS at realistic oxygen partial pressures,[11,12] although both soft[13–16] and hard[17–19] X-ray spectroscopic ex situ studies of LSM have been published. Furthermore, for lanthanum strontium cobaltite thin film electrodes an operando study applying X-ray absorption spectroscopy has been reported by Orikasa et al.[20] In general, an operando approach is very important as demonstrated in a number of studies on functional materials and structure-activity relationships, where synchrotron radiation based hard X-ray absorption spectroscopy (XAS) and X-ray emission spectroscopies (XES) have been applied (e.g. catalysis,[21–23] sensing,[24–26] batteries[27]).

An extensive operando study of LSM electrodes applying hard XAS and XES techniques has so far been missing. Hence, we report in this work how an applied electrical polarization affects the electronic structure in LSM electrodes. For this purpose, operando X-ray absorption Near Edge Structure (XANES) including High Energy Resolved Fluorescence Detection (HERFD XANES), X-ray Emission Spectroscopy (XES) and RIXS (Resonant Inelastic X-ray Scattering) techniques have been applied.

Experimental

Materials overview.—The X-ray spectroscopy reported in this study was conducted on LSM electrodes with the stoichiometric composition $(La_{0.5}Sr_{0.5})_{0.99}MnO_{3-\beta}$ (LSM50). YSZ was chosen as electrolyte material due to the good compatibility with LSM, and since the YSZ was commercially available as single crystals, serving as substrate for the deposition of LSM thin film model electrodes, as described in next section. For reference measurements MnO (99.99%), MnO_2(99.99%) and Mn_2O_3(99.99%), all from Sigma Aldrich, were employed.

Fabrication of thin film model electrodes.—For this study thin film LSM50 electrodes were used to ensure a uniform electrical polarization on dense electrodes during the experiments. Furthermore, the use of thin film model electrodes with high polarization resistance in combination with a porous composite counter electrode secured that the applied potential drop was located on thin film model electrode. Pulsed laser deposition (PLD) was used for preparation of the LSM thin film electrodes, while a YSZ single crystal served dual roles both as the electrolyte and substrate for the depositions of LSM50 film. The YSZ single crystals (CrysTeC GmbH, Germany) had a (100) exposed face, were single side polished and had the dimensions 10 mm × 10 mm × 0.5 mm. For the PLD a KrF excimer laser was used. During the deposition the fluence was 2 Jcm^{-2}, the laser frequency 10 Hz and the distance between substrate and target 7.5 cm. The LSM thin film (≈250 nm) was deposited on top of the polished side of the YSZ single crystal. The LSM deposition was conducted at a substrate temperature of 600°C and with an oxygen partial pressure of 7×10^{-4} mbar. The oxygen partial pressure was increased to 0.02 mbar immediately after the deposition and during cool-down, to avoid oxygen deficiencies developing in the LSM electrode. A "counter-electrode" consisting of a porous composite of 50% LSM and 50% $Ce_{0.9}Gd_{0.1}O_{1.95}$ (CGO) was screen-printed opposite to the LSM thin film electrode. The choice of the LSM-CGO composite electrode was made as this is a well-investigated electrode material with a fairly low resistance. After the LSM-CGO screen-printing the entire electrochemical cell was heated to 930°C for 24 h after which the thickness of the porous composite electrode was ≈30 μm. For a sketch of the sample cross-section see Figure 1.

XAS/XES measurements.—The majority of the XAS/XES measurements presented in this work were carried out at the European Synchrotron Radiation Facility (ESRF) in Grenoble, France, at the ID26 High Brilliance X-ray Spectroscopy beamline. This beamline is an undulator beamline with a high intensity. During the operando

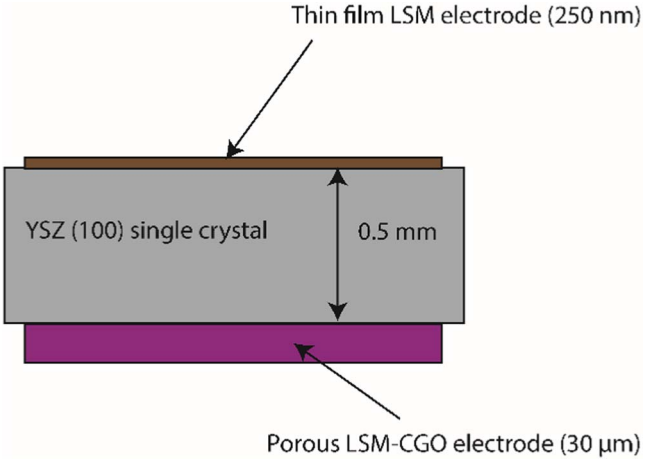

Figure 1. Schematic drawing of sample cross-section. For illustration the thickness of the individual layers are not drawn to scale.

measurements on the LSM electrodes Si (311) crystals were used for monochromation and beamsize at the sample was 75 μm * 500 μm. During the measurements on the MnO_x references Si(111) crystals were used for monochromation and beamsize at the sample was 100 μm * 500 μm. The emission spectrometer at ID26 was equipped with five Ge (620) analyzer crystals, spherically bent (r = 1 m) and installed in a Rowland geometry with respect to sample and detector.[28] An avalanche photodiode (APD) detector was used and the total energy resolution during the experiments as consequence of the lifetime broadening and the resolution of the analyzer crystals/monochromator was estimated to be better than 0.5 eV.

At each experimental condition a non-resonant X-ray emission spectrum at the Mn Kβ main lines (Kβ′ and $K\beta_{1,3}$) was recorded between 6.468 keV and 6.502 keV with stepsize 0.2 eV while applying an excitation energy of 6.700 keV.

Then HERFD XANES at the Mn K-edge were measured by scanning the incident energy across the K-edge from 6.5248 keV to 6.6251 keV with stepsize 0.1 eV, while keeping the emission energy constant at the maximum of the $K\beta_{1,3}$ line. At each investigated condition five HERFD XANES spectra were recorded and averaged prior to any further data-analysis.

Furthermore, RIXS planes were recorded around the Mn K pre-edge. The RIXS planes were recorded at open circuit voltage (OCV) and at cathodic polarizations of −500 mV, −600 mV, −700 mV and −800 mV and anodic polarizations of 500 mV and 800 mV.

Further experiments at the Sr K-edge and supplemental experiments at the Mn K-edge were conducted at the SAMBA beamline at Soleil in Saint-Aubin, France. The beamline is a bending magnet beamline, a Si(220) monochomator was used, the beamsize spot was 200 μm × 300 μm at the sample and all the measurements were conducted in fluorescence mode using a Canberra 35-element monolithic planar Ge pixel array detector. XANES spectra were measured at the Sr K-edge by scanning the energy from 15.925 keV to 16.500 keV with step size 0.3 eV, and at the Mn K-edge by scanning the energy from 6.405 keV to 6.900 keV with step size 0.2 eV.

Test conditions, experimental set-up and samples.—Two different operando studies on LSM50 electrodes were conducted. In the first study the effect of an applied potential on Mn was investigated, the study included an extensive characterization by HERFD-XANES, $K\beta_{1,3}$-XES and RIXS. This study was conducted at 500°C at 1 atm total pressure with $pO_2 = 0.2$ atm in stagnant air. The other study was conducted to compare the effect of cathodic polarization on Mn and Sr in LSM50 electrodes, this study included only XANES and was conducted at 450°C at 1 atm total pressure with $pO_2 = 0.1$ atm and balance Ar, total flowrate 50 mL/min. The differences in temperature and oxygen partial pressure between the two tests were caused by

differences in the gasses available at the beamline and a limitation in the power supply to the heat-controller. Nevertheless, the differences are insignificant for the conclusions drawn in this work. In both test cathodic potentials between −100 mV and −850 mV were applied and furthermore in the first test a few measurements with anodic potentials of 500 mV and 800 mV were made.

The establishment of the realistic test conditions simultaneously with the XAS/XES characterization was made possible due to the use of a custom-made test-house, which used a small ceramic heat-stage for sample heating and gold mesh/gold paint for current collection, the details of this testhouse have been described elesewhere.[29] A Gamry Reference 600 potentiostat was used for applying electric potentials by recording chronoamperometry curves. The temperature of the electrochemical cell during the experiments was determined from the electrolyte resistance measured by EIS combined with the temperature-resistivity expressions for YSZ given by Cheikh et al.[30]

Finally, ex situ reference XAS/XES measurements were made on pellets pressed with boron nitride and manganese oxide powders (MnO (99.99%), MnO_2(99.99%) and Mn_2O_3(99.99%)).

Data treatment and simulation.—HERFD-XANES: Five HERFD-XANES spectra recorded at each experimental condition were normalized and then averaged using the PyMca software (PyMca 4.7.3).[31] A linear fit was conducted to the pre- and postedge using OriginPro 9, and the edge energy determined as the energy halfway between the pre-edge energy and the post-edge energy

Kβ-XES:The Kβ spectra were analyzed according to the Integrals of the Absolute values of Differences (IAD) approach previously described by Rueff et al.[32] and Vanko et al.[33] Firstly, the Kβ spectra were normalized to unit area at integration in PyMca.[31] Secondly, difference plots were generated by subtracting the normalized MnO Kβ spectrum from the other Kβ spectra after which the IAD values were obtained by integration (OriginPro 9).

XANES: For XANES spectra recorded at the SAMBA beamline two spectra were recorded at each experimental condition and then averaged using the Athena interface of the IFEFFIT software package.[34]

Simulation: The XANES spectra were simulated using the Finite Difference Method Near Edge Structure (FDMNES) code by Joly.[35] Several LaSrMO4 clusters of 10 Å size were constructed. The perovskite cell parameters[36] were changed resulting in different Mn-O and Sr-O distances. Then, the calculations were carried out for each of those clusters using Green formalism. The full multiple scattering approach was employed with spherical muffin-tins potential approximation. The energy step was 0.2 eV in the pre-edge region and 0.5 eV in the edge. Finally, the simulations were used to probe the influence of the bond distances on the XANES spectra.

Results

Chronoamperometry and potential distribution in the electrochemical cell.—During the operando HERFD-XAS and XES characterization potentials in the range −850 mV to 800 mV were applied over the cell by recording chronoamperometry curves. A representative chronoamperometry curve recorded at −800 mV applied potential is shown in Figure 2. The chronoamperometry shows a pronounced degradation of the cell during the first 5 min whereafter the cell degradation rate slows down, and the cell performance becomes almost constant during the remaining part of the chronoamperometry.

For the interpretation of the results presented in the present work, the potential drop over the LSM thin film electrode is more important than the applied potential over the entire cell. However, due to the cell design with a high resistance thin film LSM electrode opposite to a low resistance composite LSM-CGO electrode, the applied potential was with a good approximation located solely as a potential drop over the LSM thin film electrode. This is supported by the impedance spectra shown in Figure 3, where Figure 3a) show the fairly low

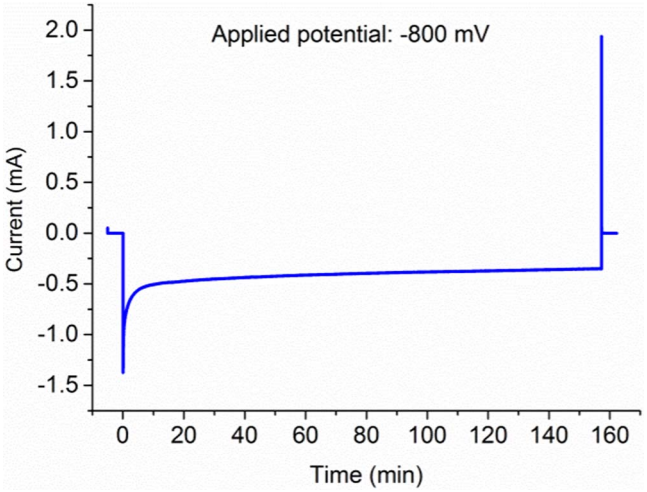

Figure 2. Representative chronoamperometry curved recorded at 500°C in $pO_2 = 0.2$ atm with a −800 mV potential applied on the cell.

resistance of cell with two porous LSM-CGO composite electrodes, while Figure 3b) show the much higher resistance for a cell with one porous LSM-CGO electrode and one LSM thin film electrode.

Operando XANES at the Mn K-edge during cathodic polarization in air.—Operando Mn K-edge X-ray absorption spectra recorded while the LSM electrode was polarized in the range 0 mV to −500 mV at 500°C did not show any effect of the applied potential on the edge position. However, applied potentials in the range −600 mV to −850 mV lead to a noticeable edge-shift, which was proportional to the magnitude of the applied potential. Figure 4 shows representative HERFD-XANES spectra recorded at various applied potentials.

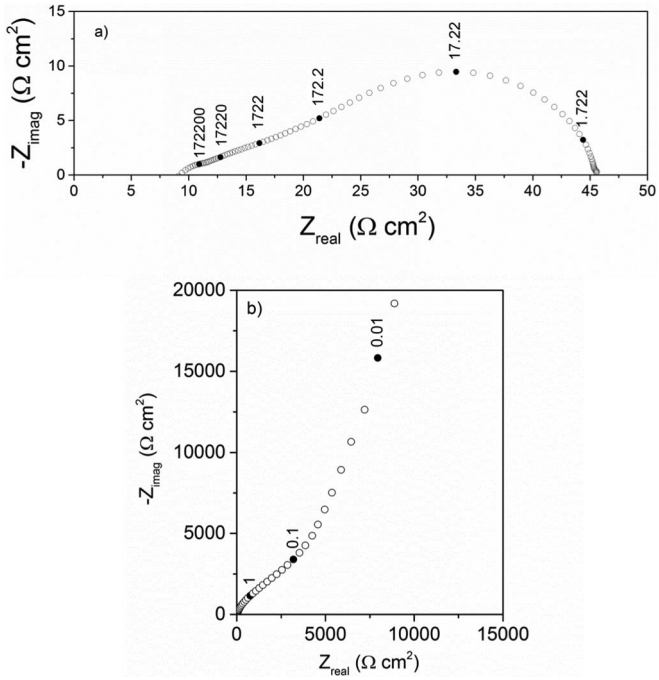

Figure 3. Impedance spectra recorded at OCV at 500°C in air on a) cell with 2 porous composite LSM-CGO electrodes and b) cell with one screen-printed LSM-CGO composite and one thin film LSM electrode. The difference in impedance response between the two cells shows that the polarization resistance of the LSM thin film electrode entirely dominates the cell polarization resistance in the latter cell.

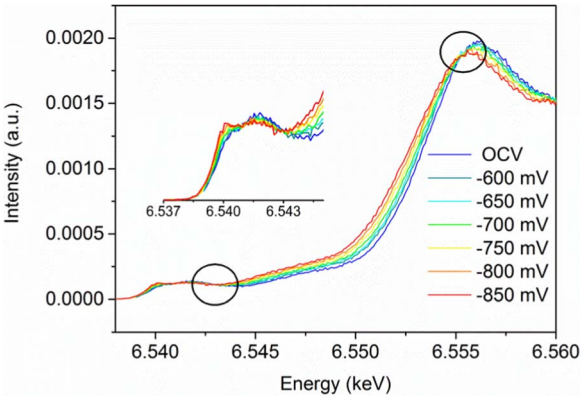

Figure 4. HERFD-XANES spectra recorded at the Mn-K edge on an LSM50 electrode at 500°C in air at OCV and with applied potentials in the range −600 mV to −850 mV. Isosbestic points are marked by black circles.

In Figure 5 a plot of the position of the Mn K-absorption edge as a function of the applied potential is depicted. Note, that the applied potentials shown e.g. in Figure 4 were not applied in order from low potentials to high potentials, but in random order. Hence, the continuous shift in the absorption edge with the applied potential is not a result from experimental drift/degradation of the sample, but a true effect from the applied potential. Overall the edge shifted by 1 eV in the investigated potential range, from ≈6.552 keV at no/low polarizations to 6.551 keV at −850 mV. This shift is obviously larger than the absolute energy resolution of less than 0.5 eV during the experiment at the ID26 beamline. Furthermore, the existence of two isosbestic points (a common intersection point for all spectra) at 6.543 keV and 6.555 keV on the HERFD-XANES suggests that the spectral changes are caused by the direct transformation of one species into another, in other words the ratio between two components appears to be changed with polarization. In addition, the cathodic polarization also caused changes in the pre-edge region at 6.533 keV-6.544 keV, cf. inset in Figure 2.

To support the interpretation of the edge shift observed in the XANES, FDMNES simulations of the spectra were conducted in which the Mn-O bond distance of the Mn-O octahedron was varied between 1.90 Å and 2.06 Å, i.e. in the vicinity of Mn-O distance reported to be 1.93–1.94 Å in literature.[37] The simulated XANES

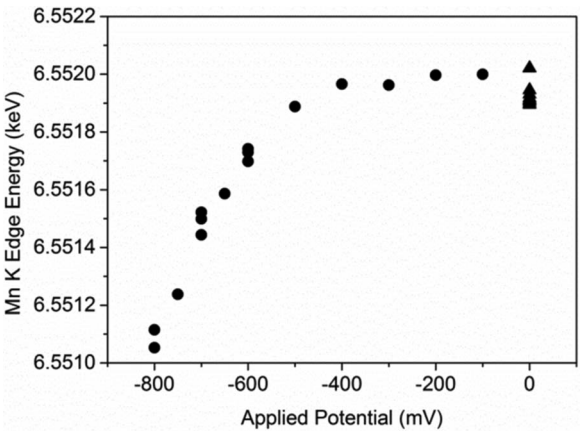

Figure 5. Mn K edge energy as function of applied potential. The triangular points at 0 mV were recorded at various times during the series of polarizations and thus reflect the scattering during the experiment. The circular data points with applied potentials include points from different measurement series, for which reason more data points are stated for some potentials. The edge energy was determined as the energy mid-way between the pre-edge and the post-edge energy.

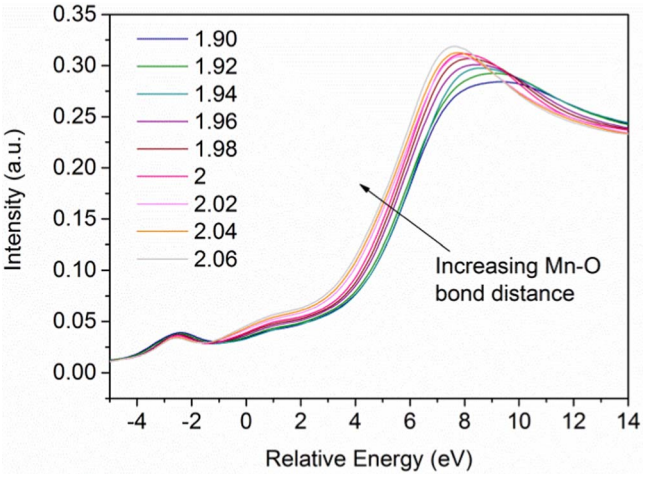

Figure 6. Simulated XANES spectra for various Mn-O bond distances of the Mn-O octahedron. The value of the Mn-O bond distance is stated in Å.

spectra presented in Figure 6 show a shift in the XANES spectra comparable to the shift observed in the experimental spectra.

Operando XANES recorded in conventional fluorescence mode at the Mn and Sr K-edge during cathodic polarization.—For comparison, conventional[e] XANES spectra without a high energy resolution fluorescence detector were recorded on the Sr K-edge of an LSM50 electrode at OCV and during cathodic polarizations, and compared to conventional Mn K-edge XANES spectra on the same electrode subjected to the same polarizations, representative results are shown in Figure 7. A cathodic polarization of −850 mV was again confirmed to cause a clear shift in the Mn K-edge (Figure 7a), while no shift and only a small shift in the shape of the edge feature was observed in the Sr K-edge Figure 7b). This is in good agreement with charge compensation during cathodic polarization and accompanying reduction of LSM electrodes being located on the Mn ions, and furthermore confirms that no strong changes in the crystal structure appears during polarization, as such changes would influence the position and shape of the Sr K-edge as well. The slight decrease in the Sr K-edge white line intensity and broadening observed in Figure 7b) is likely explained by filling of electrons into the Sr p-orbitals and increased disordering.

Mn Kβ X-ray emission data during variation of the applied potential.—In addition to HERFD-XANES spectra also XES data at the Mn Kβ main emission lines ($K\beta_{1,3}$ and $K\beta'$) were collected both on the MnO_x reference samples ex situ and on the LSM50 electrode while it was subjected to various applied potentials at 500°C (Figure 8). To highlight the effect of the applied potential on the LSM50 electrode the IAD values were calculated and compared between the references and the LSM50 electrode (Figure 9). The IAD values for the MnO_x references show a linear dependency on the oxidation state with an R^2-value 0.99 (Figure 9). When comparing the IAD values of LSM electrodes obtained in the range of applied potentials from 0 mV to −800 mV to the IAD values of the MnO_x references, a decrease in average Mn oxidation state from 3.4 to 3.2 was obtained (Figure 9).

Resonant inelastic X-ray scattering.—RIXS planes around the Mn K pre-edge were recorded on the three MnO_x references (Figure 10). The pre-edge (corresponding to 1*s* spin-down transitions to empty 3*d* levels) is visible as a clear feature at an energy transfer of

[e]Conventional in this context refers to the energy resolution corresponding to the core-hole lifetime broadening of the K-electrons, as all Fluorescence X-rays are in a range of 100–150 eV in these spectra, in contrast to the high energy resolution XANES recorded at the ID26 beamline.

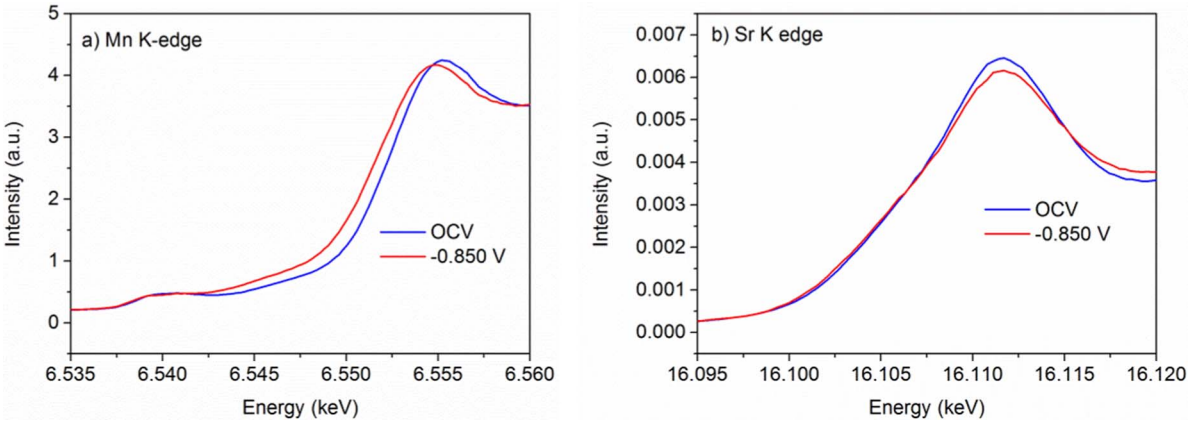

Figure 7. Comparison between edge shifts on K edges of a) Mn and b) Sr when −0.85 V polarization is applied on LSM50 electrodes in 10% O_2 at 450°C.

≈50 eV, labelled with "A" in Figures 10a–10c. Furthermore, on the RIXS planes of Mn_2O_3 (Mn^{3+}, [Ar]$3d^4$) and MnO_2 (Mn^{4+},[Ar]$3d^3$) a second "peninsula –like" feature is visible at an energy transfer of ≈65 eV, this feature is marked by "B" in Figures 10b and 10c. The "B" feature is assigned to spin-up transitions[38,39] and will be discussed further in the section Probing polarization induced changes in the 3d configuration of Mn by RIXS.

On the RIXS planes recorded on LSM electrode at 500°C and OCV (Figure 11a), both the spin-down transition ("A") and the spin-up transition ("B") features observed for the MnO_x references were visible. With an increase in the magnitude of the applied cathodic potential on the LSM electrode, the spin-up transition ("B") feature was clearly weakened (Figures 11b–11d).

To emphasize the effect of the polarization on the spin-down transition ("A") and the spin-up transition ("B"), plots that show the intensity of the emitted energy as function of the incident energy for the A and B-feature separately are depicted in Figure 12. In this figure the plots for the A feature are based on the intensity counted by the detector due the emitted photons with an energy between 6.485–6.495 keV and for the B feature the corresponding energy of 6.470 keV–6.480 keV was used. While the cathodic polarization reduces the intensity of the spin-up transition ("B") the spin-down transition ("A") is both reduced in intensity and changing its shape with cathodic polarization, as also evident in the HERFD-XANES spectra previously described.

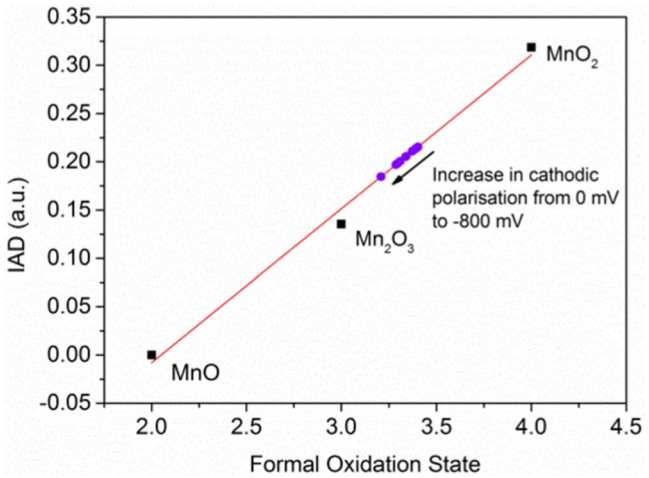

Figure 9. Integrals of the absolute values of the difference spectra (IAD) for the Mn Kβ main emission lines for MnO_x reference powders (black squares) and for the LSM50 electrode at 500°C at applied potentials in the range 0 mV to −800 mV (violet circles). The dashed line marks the linear fit to the IAD values of the three MnO_x reference compounds.

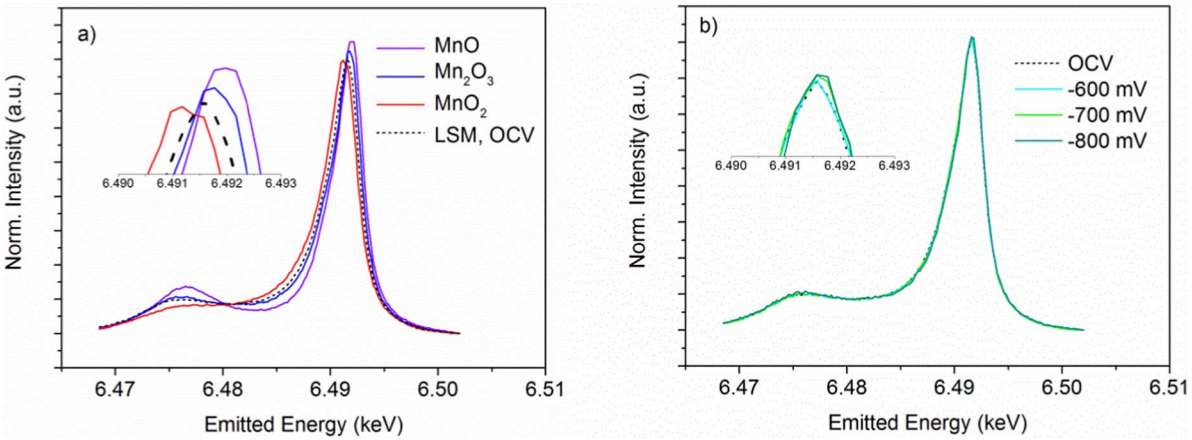

Figure 8. Representative Mn Kβ main emission lines at excitation energy 6.700 keV, a) ex situ on MnO_x samples and b) on LSM50 electrode at 500°C while subjected to potentials of −600 mV, −700 mV and −800 mV. In both a) and b) the same spectrum for the LSM50 electrode at 500°C and OCV is shown for comparison.

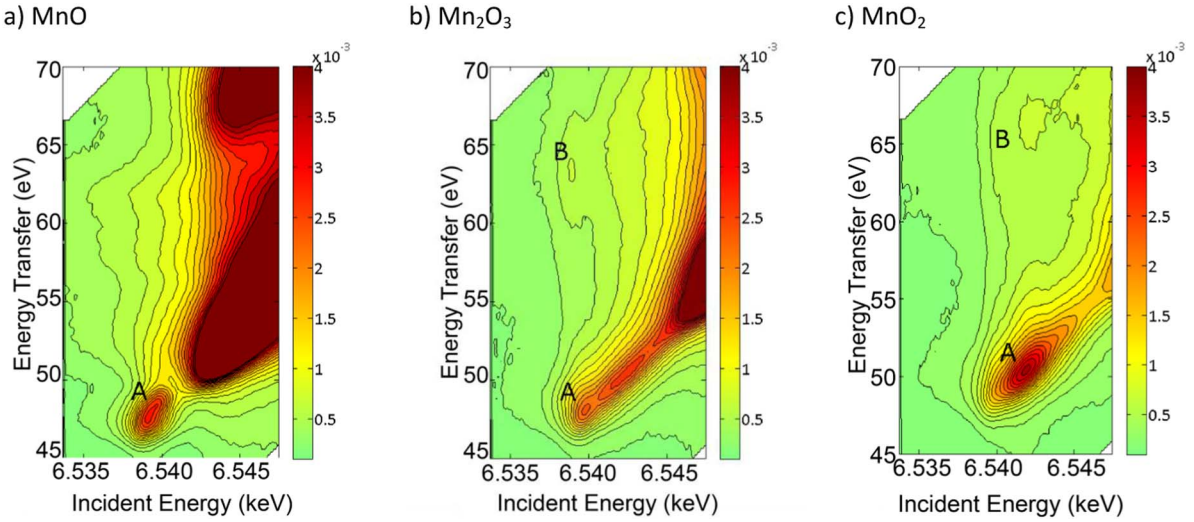

Figure 10. RIXS planes recorded at the Mn K pre-edge at RT on powder reference samples of a) MnO (Mn^{2+}), b) Mn_2O_3 (Mn^{3+}) and c) MnO_2 (Mn^{4+}).

Discussion

In the previous section the results from various measurements (Mn K-edge HERFD-XANES, Kβ-XES and RIXS and fluorescence XAS at the Mn K- and Sr K-edge) on LSM50 electrodes were presented together with measurements on MnO_x references. For the LSM50 electrode spectra were recorded at OCV, under cathodic polarizations between −100 mV and −850 mV and under anodic polarizations of 500 mV and 800 mV. A general observation from the majority of the measurements was that anodic polarizations and cathodic polarisations with a magnitude below −600 mV did not have a detectable effect. Yet applied polarizations in the range −600 mV to −850 mV led to detectable changes in the electronic structure around the Mn. In this section an interpretation of these changes will be discussed by combining the results of the presented measurements.

Mn reduction and associated LSM lattice expansion observed at the Mn K pre-edge and main-edge.—The Mn K edge shows an evident and consistent shift toward lower energies when potentials in the range −600 mV to −850 mV are applied. Traditionally, a shift in the K-edge has been interpreted as a sign of oxidation state changes,

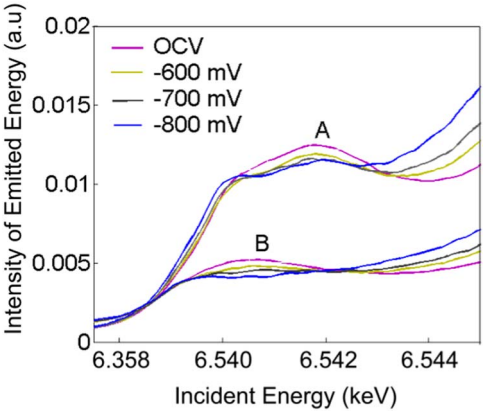

Figure 12. The number of emitted photons as function of the incident energy at the Mn K pre-edge. "A" plots were generated from the emitted photons with an energy between 6.485–6.495 keV and are related to spin-down transition, while "B" plots were generated from the emitted photons with an energy between 6.470–6.480 keV and are related to spin-up transitions.

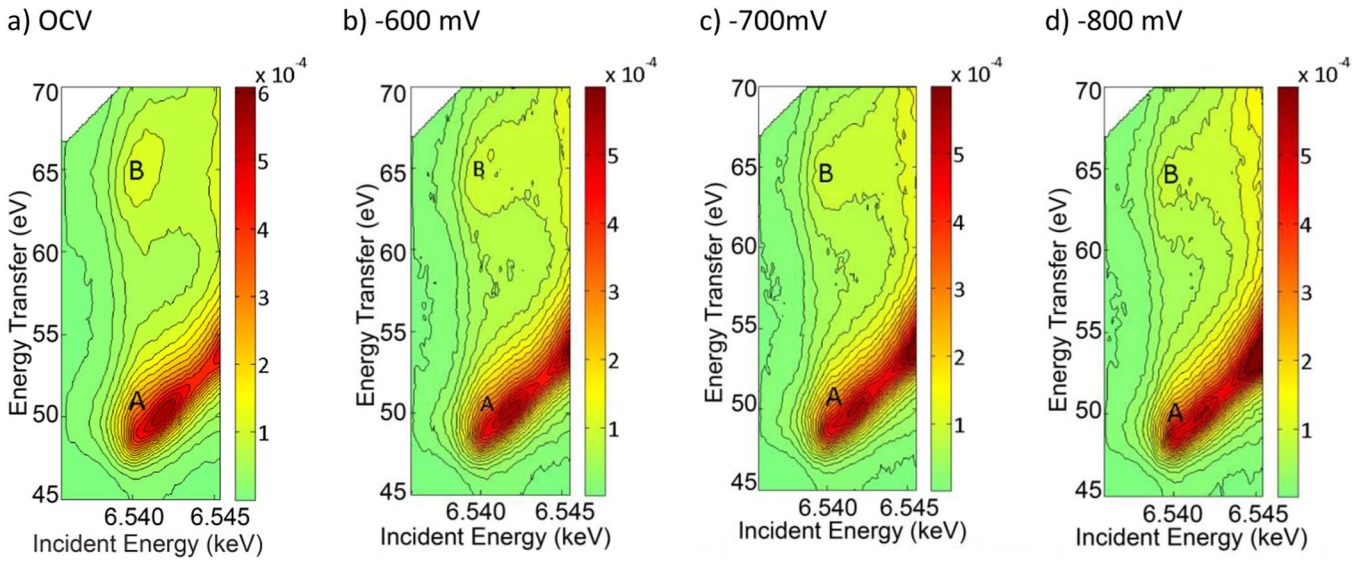

Figure 11. RIXS planes recorded on LSM50 electrode at 500°C in air while the electrode was subjected to a) OCV, b) −600 mV, c) −700 mV and d) −800 mV.

yet it has also been known for long, that the edge shift by large was correlated to the change in bond distance associated with oxidation state changes (cf. Glatzel et al. 2009[40]). This is in agreement with conducted FDMNES calculations in this work which shows a shift in the simulated Mn K-edge with Mn-O bond distances comparable to the ones observed in the experimental XANES spectra. An unambiguous assignment of the edge energy to a specific oxidation state must be made with care, as the edge energy also depends on coordination geometry and the ligands.[41] However, in the present case, where the XANES data are recorded on the same sample subjected to different polarizations, the edge shift can rather not be attributed to a change in ligands. It is more likely a sign of an overall reduction in the Mn oxidation state, caused by a polarization induced increase in the number of oxygen vacancies. This is consistent with an associated expansion in the LSM lattice previously detected by operando by XRD.[42] In this connection it is worthwhile mentioning, that the number of oxygen vacancies created in LSM50 at 500°C and −0.8V polarization is expected to be approx. 5% of the total number of oxygen vacancies (see Appendix), thus no major symmetry changes are expected around the Mn ions in the structure. The lack of symmetry changes is furthermore supported by the fact that no shift and hardly any changes in the shape of the Sr K-edge were observed.

The reduction in the Mn oxidation state and the accompanying changes in the electronic structure is also qualitatively reflected in the in the changes in the Mn K pre-edge as visible both in the HERFD-XANES and the RIXS planes. However, in this work the correlation between Mn oxidation state and the pre-edge was not explored further, but this could be considered in the future following a similar procedure as described by Farges.[41]

Quantification of polarization induced Mn oxidation state change by Kβ XES.—The XES of the Mn Kβ main lines show only minor changes upon cathodic polarization, thus hardly any changes in spin state were observed.[33] The accompanying IAD analysis shows a decrease in the average Mn oxidation state for LSM50 from 3.4 at OCV to 3.2 at −0.8 V polarization. It is of interest to compare these experimentally determined oxidation states to those predicted by Mizusaki et al.[6] Based on the work by Mizusaki et al. it was calculated that if the electrical polarization is changed from OCV to −0.8 V at 500°C, the average Mn oxidation state should change from 3.5 to 3.2 for LSM50 (See Appendix for the calculation). Even though Mizusaki theoretically predicted the average Mn oxidation state for LSM50 at OCV to be 3.5, he observed experimentally by thermogravimetry only values of 3.3–3.4[6]. The change in the average Mn oxidation state upon cathodic polarization determined experimentally in this work is thus in very good agreement with the expected average Mn oxidation state predicted by Mizusaki et al.[6] However, when it comes to predicting concentration of the individual Mn^{2+}, Mn^{3+} and Mn^{4+}, the work by Mizusaki et al. is not supported with the present experimental findings. This will be discussed further in the section Changes in Mn^{2+}, Mn^{3+} and Mn^{4+} concentrations during polarization – evidence of only two components changing.

Probing polarization induced changes in the 3d configuration of Mn by RIXS.—RIXS planes recorded around the Mn K- pre-edge of both the MnO_X references and the LSM50 electrodes subjected to various polarizations at 500°C were presented in the results section. The most noticeable difference between the RIXS planes of the MnO_x references is a feature (feature "B") at an energy transfer of 65 eV (Figure 10) which is not present for MnO (Mn^{2+}) but evident for Mn_2O_3 (Mn^{3+}) and MnO_2 (Mn^{4+}). This feature has previously been observed on RIXS planes of manganese oxides[38] and iron oxides,[43] and assigned to spin up transitions.[38,39] The explanation in more detail is the following:[38,39] For Mn^{2+} all the 3*d* orbitals contain one electron in a spin-up state (high spin case), allowing only spin-down transitions during the excitation of the 1*s* electron to the 3*d* orbitals. Subsequently, only one relaxation pathway (spin down) is possible for the 3*p* orbital electron to the hole in the 1*s* orbital. With higher Mn oxidation states (Mn^{3+} and Mn^{4+}) one or more of the 3*d* orbitals is empty, and thus both spin-down and spin-up transitions are possible, the latter giving rise to the feature "B" observed at energy transfer 65 eV (Figure 10). For the RIXS planes of the LSM electrodes subjected to various cathodic polarizations it is evident, how the spin-up feature (feature "B") is weakened with increasing cathodic polarization. This is reasonably interpreted by the cathodic polarization leading to a reduction of the manganese ions from $3d^3$ configuration to $3d^4$ configuration, keeping in mind the HERFD-XANES indicated no Mn^{2+} ($3d^5$ configuration) was formed as only two components changed during polarization. The filling of the *d* orbitals during cathodic polarization leads to the decrease in the number of spin-up transitions observed on the RIXS planes.

Changes in Mn^{2+}, Mn^{3+} and Mn^{4+} concentrations during polarization – evidence of only two components changing.—The overall assumption by Mizusaki et al.[6] and other groups[44] is that charge compensation during cathodic polarization/creation of oxygen vacancies in LSM is achieved by a reduction in average Mn oxidation state. This is experimentally confirmed by the results from the operando HERFD-XANES, the Kβ XES and the RIXS techniques in this work.

Regarding the concentration of the individual Mn ions in the LSM50 electrodes, extrapolation of the results from Mizusaki et al.[6] from 600–1000°C to 500°C lead to calculated concentrations at −0.8 V of $[Mn^{2+}] = 0.17$, $[Mn^{3+}] = 0.49$ and $[Mn^{4+}] = 0.34$ (the values are stated as the fractions on the Mn sites, for the calculation see Appendix). In contrast to this, recent DFT calculations by Pavone et al.[5] suggested that for LSM50 charge balance during cathodic polarization/creation of oxygen vacancies would be obtained solely by reduction of Mn^{4+} to Mn^{3+}, i.e. no formation of Mn^{2+} would be involved. In this experimental work, the presence of isosbestic points in the HERFD-XANES evidence only two components, presumably Mn^{4+} and Mn^{3+}, that change their ratio during cathodic polarization. Thus the experiments conducted in this work confirm the DFT based predictions by Pavone et al.[5], that the effect of cathodic polarization on LSM50 electrodes is a reduction of Mn^{4+} to Mn^{3+} prior to any significant further reduction to Mn^{2+}.

In summary, this operando study confirms predictions regarding reduction in manganese oxidation state and formation of oxygen vacancies in LSM during cathodic polarization, predictions which to a large extent have been based on indirect measurements (thermogravimetry, electrochemical characterization)[4,6,45] and primarily have been investigated in situ by means of techniques like XPS which have required vacuum environment far from the real operating conditions of LSM electrodes.[4,46] Moreover, the present study gives a quantitative estimation of manganese oxidation state in the bulk LSM, making it possible to compare to predictions from defect models and DFT calculations. Note that the penetration depth of the hard X-rays applied allows real operando studies, but due the high energy of the hard X-rays the whole thickness of the applied LSM electrode (250 nm) is penetrated and thus the Mn oxidation state is probed through the entire LSM thin film in the present study. Despite of the differences in pressure, both this study and previous surface sensitive in situ XPS studies[4,46] observe the polarization induced reduction in manganese oxidation state. A future point which would be of interest to investigate operando in more detail is the observation of heterogeneity between the LSM bulk and surface, as already evident from ex situ,[47] in situ[8] and operando studies.[11] For such studies grazing incidence experiments would be of great value. Finally an important perspective of this work is, that operando XANES, XES and RIXS could be employed to other less investigated perovskites applied as air electrodes in solid oxide cells. A reduction in manganese oxidation state during cathodic polarization as observed in this work is expected for the LSM perovskite, yet for many other less investigated perovskites ($La_{0.6}Sr_{0.4}Co_{0.2}Fe_{0.8}O_3$, $Pr_{0.6}Sr_{0.4}Co_{0.2}Fe_{0.8}O_3$, $LaNi_{0.6}Fe_{0.4}O_3$ among others) it is less clear which element will change oxidation state during cathodic polarization. For these less investigated perovskites, the used element-sensitive techniques of the present study would be of beneficial use.

Conclusions

The application of novel hard X-ray spectroscopic techniques (HERFD-XAS, XES, RIXS) for determining structure-function relationships has been demonstrated to be a powerful approach for studying electrocatalysts like LSM used for the OER and ORR in air electrodes. This extends the application of these techniques from minerals,[48,49] transition metal complexes,[50] sensing,[24–26] batteries[27] and working catalysts,[51–54] for which they have already been proven to be sensitive tools for determining the oxidation state and coordination.

HERFD-XANES, Kβ XES and RIXS studies were successfully conducted at 500°C in 10–20% O_2 with application of anodic and cathodic polarizations on the LSM50 electrode. While anodic polarizations and cathodic polarizations lower than −500 mV did not influence the electronic structure in a measurable manner, cathodic polarizations in the range −600 mV to −850 mV lead to profound changes in the electronic structure/Mn oxidation states. The larger the magnitude of the cathodic polarization the more pronounced were the observed changes in HERFD-XANES (pre-edge feature, edge position), XES (slight changes due to reduction) and RIXS (spin up/spin down features). The cathodic polarization caused a reduction in the average Mn oxidation state from about 3.4 at OCV to 3.2 at −800 mV. During cathodic polarization and accompanying Mn reduction electrons were donated into the Mn 3*d* orbitals. Furthermore, the reduction during cathodic polarization led to the change in the ratio of only two components, most likely Mn^{3+} and Mn^{4+}. The average Mn oxidation state changes observed experimentally in this work are in good agreement with predictions based on the work by Mizusaki et al.[6] while the observed change in Mn ion ratios are in good agreement with DFT based predictions by Pavone et al.[5]

This shows that operando studies using hard X-rays are very attractive and will be an important tool in future for obtaining further detailed understanding of the interplay between electrical polarization and the ORR and OER. For this reason other electrocatalyst than LSM, both perovskites and other structures, should be investigated further with these element-sensitive operando techniques.

Acknowledgment

The operando HERFD-XANES, Kβ XES and RIXS experiments were performed on beamline ID26 at the European Synchrotron Radiation Facility (ESRF), Grenoble, France. We are grateful to Pieter Glatzel and Kristina Kvashnina at the ESRF for their help at beamline ID26. XANES with a solid state fluorescence detector was performed on SAMBA beamline at Soleil, Saint-Aubin, France. We are grateful to Emiliano Fonda and Guillaume Alizon at Soleil for providing assistance in using the SAMBA beamline. At DTU Energy Jens Borchsenius is acknowledged for assisting in the testhouse construction and Simone Sanna for assisting with the sample preparation. This work was supported by the Danish Independent Research Council - Technology and Production, project no. 12-131965 and synchrotron radiation experiments by ESRF and SOLEIL.

Appendix

In the present study the prediction of theoretical oxidation states of Mn and oxygen non-stoichiometry δ upon polarization of LSM ($La_{1-x}Sr_xMnO_{3\pm\delta}$) electrodes is based on the experimental and theoretical work described in the paper "Oxygen nonstoichiometry and defect equilibrium in the perovskite-type oxides $La_{1-x}Sr_xMnO_{3+\delta}$" by Mizusaki et al.[6] The work by Mizusaki et al. contains experimental non-stoichiometry curves for LSM, where the oxygen non-stoichiometry *d* is stated as a function of Sr substitution level (x_{sr} = [0.1; 0.5]), temperature (T = [600°C; 1000°C]) and oxygen pressure (pO_2 = [10^{-20}atm; 1 atm]). Furthermore the work contains theoretical estimations of the population of the individual Mn ions calculated from defect modelling.

To correlate the electrical polarization applied in the present work to the apparent oxygen partial pressure in the electrode, the LSM thin film electrode is considered an oxygen pump, pumping oxygen from the electrode surface toward the electrolyte during cathodic polarization. In this case, the relationship between oxygen partial pressure at the electrode surface p_{ref} and the apparent oxygen partial pressure in the electrode p'_{O2} due to the polarization is given by the expression

$$E = \frac{RT}{4F} \ln \frac{p'_{O_2}}{p_{ref}} \quad [A1]$$

in which *E* is the potential difference/the electrical polarization over the LSM electrode, *R* is the gas constant, *T* is the temperature and *F* is the Faraday constant. For comparison to the polarization experiments on LSM50 p_{ref} = 0.2 atm was used.

By inserting cathodic polarizations in the range −0.5 V to −0.8 V in equation A1, the corresponding apparent partial pressure in the electrode p'_{O2} is calculated, and from the non-stochiometry curve for LSM50 (Mizusaki et al. Figure 6) the associated oxygen non-stoichiometry *d* is derived. The *d* values determined in this way are shown in Figure A1. Even though linear dependency cannot in general be expected for plots of oxygen non-stoichiometry curves vs. temperature, a linear fit could be justified for the −0.7 V data and −0.8 V data, yielding R^2 values of 1.00 and 0.97 respectively.

From the linear fits extrapolations were made to obtain the δ-values at 500°C, which are stated in Table AI. In Table AI is furthermore stated average Mn oxidation state and the concentration of the individual Mn-ions calculated according to Mizusaki et al.[6]

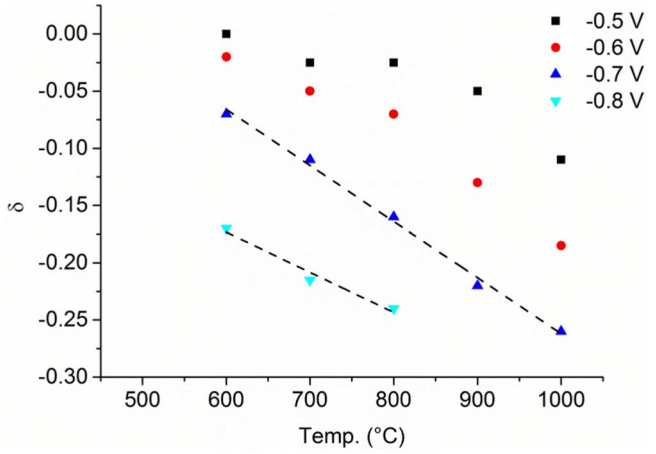

Figure A1. Oxygen nonstochiometry δ as function of temperature and applied electrical polarization. Values are determined by combining results from Mizusaki et al.[6] with Equation A1 stated above. Dashed lines show linear fit of the dataseries for −0.7V and −0.8 V.

Table AI. The table contains estimations of oxygen non-stochiometry and Mn oxidation states calculated from the results of Mizusaki et al. for LSM50 at 500°C. The number of oxygen vacancies is stated both as δ values and as percentage of the total number of oxygen sites. Together with the average Mn oxidation state the concentration of the individual Mn ions is stated as the fraction of the total number of Mn sites, calculated according to Mizusaki et al.

Applied potential [V]	δ at 500°C	Oxygen vacancies [%]	Average Mn oxidation state	$[Mn^{2+}]$	$[Mn^{3+}]$	$[Mn^{4+}]$
0	0	0	3.50	0	0.50	0.50
−0.7	−0.02	0.7	3.46	0	0.54	0.46
−0.8	−0.16	5.4	3.17	0.17	0.49	0.34

References

1. C. W. Sun, R. Hui, and J. Roller, *J. Solid State Electrochem.*, **14**, 1125 (2010).
2. S. P. Jiang, *J. Mater. Sci.*, **43**, 6799 (2008).
3. A. Hammouche, E. Siebert, A. Hammou, M. Kleitz, and A. Caneiro, *J. Electrochem. Soc.*, **138**, 1212 (1991).
4. H. Y. Lee, W. S. Cho, S. M. Oh, H. D. Wiemhofer, and W. Gopel, *J. Electrochem. Soc.*, **142**, 2659 (1995).
5. M. Pavone, A. B. Muñoz-García, A. M. Ritzmann, and E. A. Carter, *J. Phys. Chem. C.*, **118**, 13346 (2014).
6. J. Mizusaki, N. Mori, H. Takai, Y. Yonemura, H. Minamiue, H. Tagawa, M. Dokiya, H. Inaba, K. Naraya, T. Sasamoto, and T. Hashimoto, *Solid State Ionics.*, **129**, 163 (2000).
7. M. Backhaus-Ricoult, K. Adib, T. St. Clair, B. Luerssen, L. Gregoratti, and A. Barinov, *Solid State Ionics.*, **179**, 891 (2008).

8. A. Huber, M. Falk, M. Rohnke, B. Luerssen, M. Amati, L. Gregoratti, D. Hesse, and J. Janek, *J. Catal.*, **294**, 79 (2012).
9. H. Jalili, J. W. Han, Y. Kuru, Z. Cai, and B. Yildiz, *J. Phys. Chem. Lett.*, **2**, 801 (2011).
10. D. N. Mueller, M. L. Machala, H. Bluhm, and W. C. Chueh, *Nat. Commun.*, **6**, 6097 (2015).
11. K. Chang, B. Yildiz, D. J. Myers, J. D. Carter, and H. You, *ECS Trans*, **16**(51), 23 (2009).
12. Y. Orikasa, T. Ina, T. Nakao, T. Fukutsuka, A. Mineshige, K. Amezawa, T. Kawada, and Y. Uchimoto, *Meet. Abstr.- Electrochem.Soc.*, **1001**, 531 (2010).
13. M. Abbate, F. M. F. de Groot, J. C. Fuggle, A. Fujimori, O. Strebel, F. Lopez, M. Domke, G. Kaindl, G. A. Sawatzky, M. Takano, Y. Takeda, H. Eisaki, and S. Uchida, *Phys. Rev. B.*, **46**, 4511 (1992).
14. M. de Jong, I. Bergenti, W. Osikowicz, R. Friedlein, V. Dediu, C. Taliani, and W. Salaneck, *Phys. Rev. B.*, **73**, 52403 (2006).
15. L. F. J. Piper, A. R. H. Preston, S. -W. Cho, A. DeMasi, B. Chen, J. Laverock, K. E. Smith, L. J. Miara, J. N. Davis, S. N. Basu, U. Pal, S. Gopalan, L. Saraf, T. Kaspar, A. Y. Matsuura, P. -A. Glans, and J. -H. Guo, *J. Electrochem. Soc.*, **158**, B99 (2011).
16. T. Noh and H. Lee, *J. Solid State Electrochem.*, **18**, 613 (2014).
17. S. M. Mini, J. F. Mitchell, D. G. Hinks, A. Alatas, D. Rosenmann, C. W. Kimball, and P. A. Montano, *Science and Technology of Magnetic Oxides*, **494**, 59 (1998).
18. T. Shibata, B. Bunker, J. F. Mitchell, and P. Schiffer, *Phys. Rev. Lett.*, **88**, 207205 (2002).
19. C. Yunphuttha, S. Porntheeraphat, A. Wongchaisuwat, S. Tangbunsuk, D. W. M. Marr, and P. Viravathana, *Phys. Chem. Chem. Phys.*, **18**, 16786 (2016).
20. Y. Orikasa, E. J. Crumlin, S. Sako, K. Amezawa, T. Uruga, M. D. Biegalski, H. M. Christen, Y. Uchimoto, and Y. Shao-Horn, *ECS Electrochem. Lett.*, **3**, F23 (2014).
21. P. Glatzel and U. Bergmann, *Coord. Chem. Rev.*, **249**, 65 (2005).
22. J. -D. Grunwaldt, *J. Phys. Conf. Ser.*, **190**, 012151 (2009).
23. J. Singh, C. Lamberti, and J. A. van Bokhoven, *Chem. Soc. Rev.*, **39**, 4754 (2010).
24. A. Gurlo and R. Riedel, *Angew. Chem. Int. Edit.*, **46**, 3826 (2007).
25. D. Koziej, M. Huebner, N. Barsan, U. Weimar, M. Sikora, and J. -D. Grunwaldt, *Phys. Chem. Chem. Phys.*, **11**, 8620 (2009).
26. M. Huebner, D. Koziej, M. Bauer, N. Barsan, K. Kvashnina, M. D. Rossell, U. Weimar, and J. -D. Grunwaldt, *Angew. Chem. Int. Edit.*, **50**, 2841 (2011).
27. J. McBreen, *J. Solid State Electrochem.*, **13**, 1051 (2009).
28. G. Vanko, A. Bordage, P. Glatzel, E. Gallo, M. Rovezzi, W. Gawelda, A. Galler, C. Bressler, G. Doumy, A. M. March, E. P. Kanter, L. Young, S. H. Southworth, S. E. Canton, J. Uhlig, G. Smolentsev, V. Sundstrom, K. Haldrup, T. B. van Driel, M. M. Nielsen, K. S. Kjaer, and H. T. Lemke, *J. Electron. Spectrosc. Relat. Phenom.*, **188**, 166 (2013).
29. M. L. Traulsen, *J. Phys. Conf. Ser.*, **499**, 012010 (2014).
30. A. Cheikh, A. Madani, A. Touati, H. Boussetta, and C. Monty, *J. Eur. Ceram. Soc.*, **21**, 1837 (2001).
31. V. A. Sole, E. Papillon, M. Cotte, P. Walter, and J. Susini, *Spectrochim. Acta, Part B.*, **62**, 63 (2007).
32. J. P. Rueff, A. Shukla, A. Kaprolat, M. Krisch, M. Lorenzen, F. Sette, and R. Verbeni, *Phys. Rev. B.*, **63**, 132409 (2001).
33. G. Vanko, T. Neisius, G. Molnar, F. Renz, S. Karpati, A. Shukla, and F. M. F. de Groot, *J. Phys. Chem. B.*, **110**, 11647 (2006).
34. B. Ravel and M. Newville, *J. Synch. Rad.*, **12**, 537 (2005).
35. Y. Joly, *Phys. Rev. B.*, **63**, 125120 (2001).
36. J. Dhahri, S. Zemni, K. Cherif, J. Dhahri, M. Oumezzine, A. Ghedira, and H. Vincent, *J. Alloys Compounds.*, **394**, 51 (2005).
37. P. Woodward, T. Vogt, D. Cox, A. Arulraj, C. Rao, P. Karen, and A. Cheetham, *Chem. Mat.*, **10**, 3652 (1998).
38. H. Hayashi, M. Kawata, R. Takeda, Y. Udagawa, Y. Watanabe, T. Takano, S. Nanao, and N. Kawamura, *J. Electron. Spectrosc. Relat. Phenom.*, **136**, 191 (2004).
39. K. Hämäläinen, C. C. Kao, J. B. Hastings, D. P. Siddons, L. E. Berman, V. Stojanoff, and S. P. Cramer, *Phys.Rev.B.*, **46**, 14274 (1992).
40. P. Glatzel, G. Smolentsev, and G. Bunker, *J. Phys. Conf. Ser.*, **190**, 012046 (2009).
41. F. Farges, *Phys. Rev. B.*, **71**, 155109 (2005).
42. L. Sorby, F. Poulsen, H. Poulsen, S. Garbe, and J. Thomas, *Mater. Sci. Forum.*, **278**, 408 (1998).
43. G. D. Pirngruber, J. Grunwaldt, J. A. van Bokhoven, A. Kalytta, A. Reller, O. V. Safonova, and P. Glatzel, *J. Phys. Chem. B.*, **110**, 18104 (2006).
44. J. H. Kuo, H. U. Anderson, and D. M. Sparlin, *J. Solid State Chem.*, **83**, 52 (1989).
45. A. Hammouche, E. Siebert, A. Hammou, M. Kleitz, and A. Caneiro, *J. Electrochem. Soc.*, **138**, 1212 (1991).
46. M. Backhaus-Ricoult, K. Adib, T. S. Clair, B. Luerssen, L. Gregoratti, and A. Barinov, *Solid State Ionics.*, **179**, 891 (2008).
47. K. Norrman, K. V. Hansen, and T. Jacobsen, *RSC Advances.*, **5**, 87679 (2015).
48. M. Wilke, F. Farges, P. E. Petit, G. E. Brown, and F. Martin, *Am. Mineral.*, **86**, 714 (2001).
49. P. Glatzel, A. Mirone, S. G. Eeckhout, M. Sikora, and G. Giuli, *Phys. Rev. B.*, **77**, 115133 (2008).
50. G. Smolentsev, A. V. Soldatov, J. Messinger, K. Merz, T. Weyhermueller, U. Bergmann, Y. Pushkar, J. Yano, V. K. Yachandra, and P. Glatzel, *J. Am. Chem. Soc.*, **131**, 13161 (2009).
51. J. -D. Grunwaldt and B. Clausen, *Top. Catal.*, **18**, 37 (2002).
52. J. -D. Grunwaldt, B. Kimmerle, A. Baiker, P. Boye, C. G. Schroer, P. Glatzel, C. N. Borca, and F. Beckmann, *Catal. Today.*, **145**, 267 (2009).
53. S. Bordiga, E. Groppo, G. Agostini, J. A. van Bokhoven, and C. Lamberti, *Chem. Rev.*, **113**, 1736 (2013).
54. A. Boubnov, H. W. P. Carvalho, D. E. Doronkin, T. Guenter, E. Gallo, A. J. Atkins, C. R. Jacob, and J. -D. Grunwaldt, *J. Am. Chem. Soc.*, **136**, 13006 (2014).